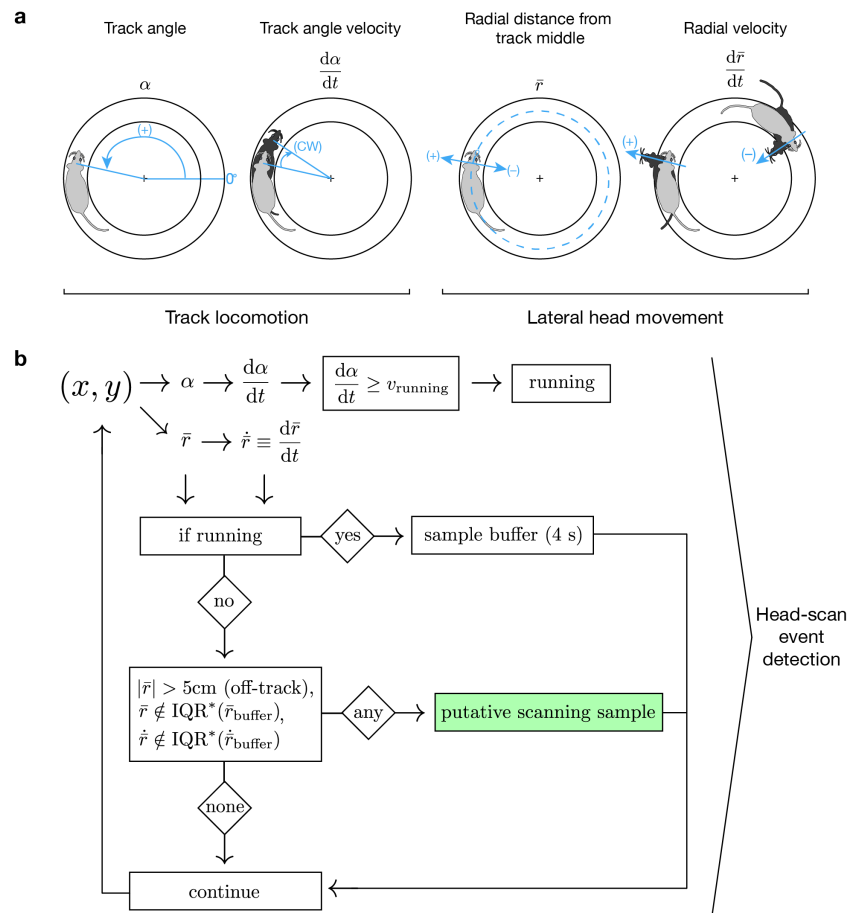


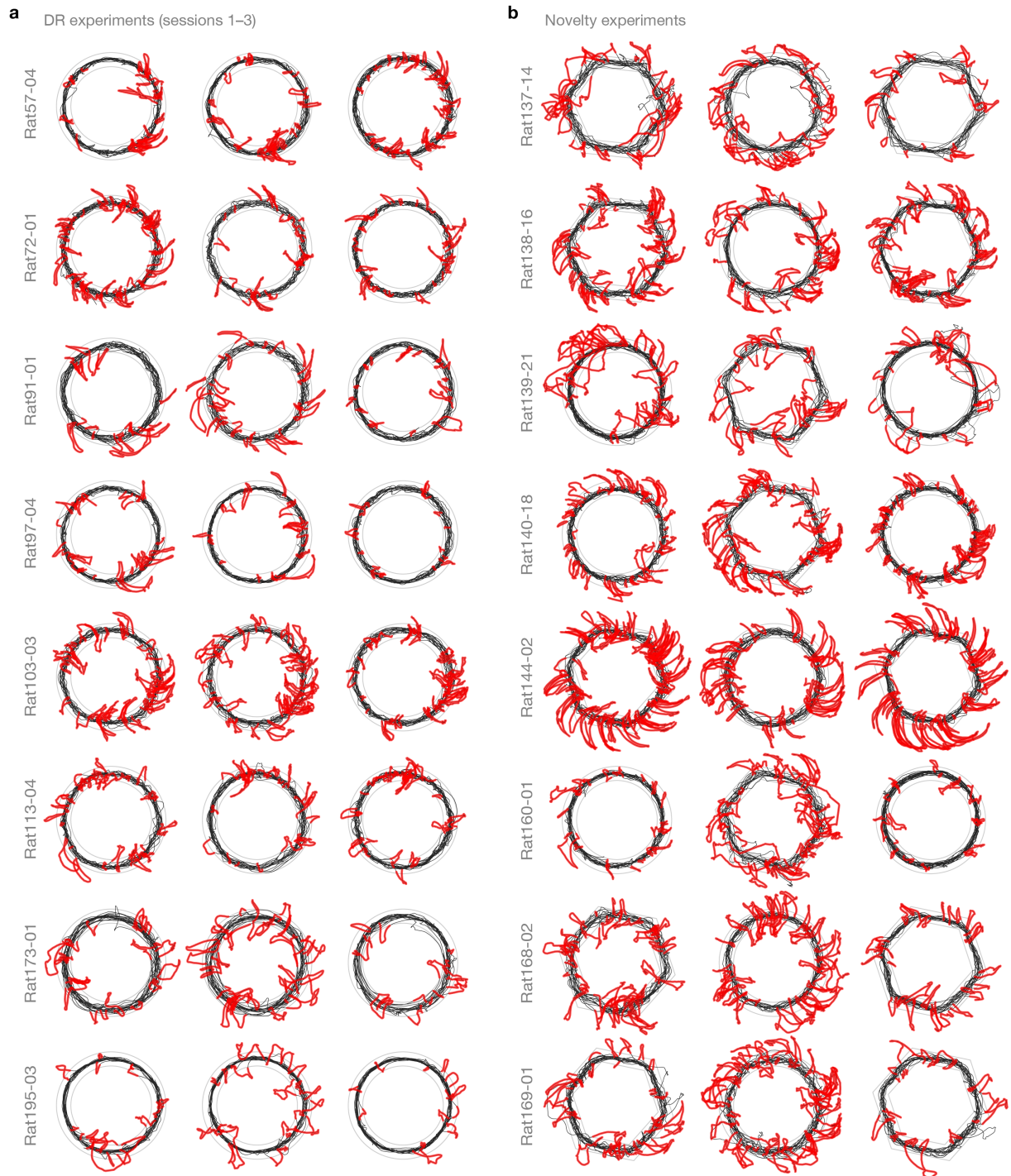
Supplementary Information | Attentive Scanning Behavior Drives One-Trial Potentiation of Hippocampal Place Fields

Joseph D. Monaco, Geeta Rao, Eric D. Roth, and James J. Knierim

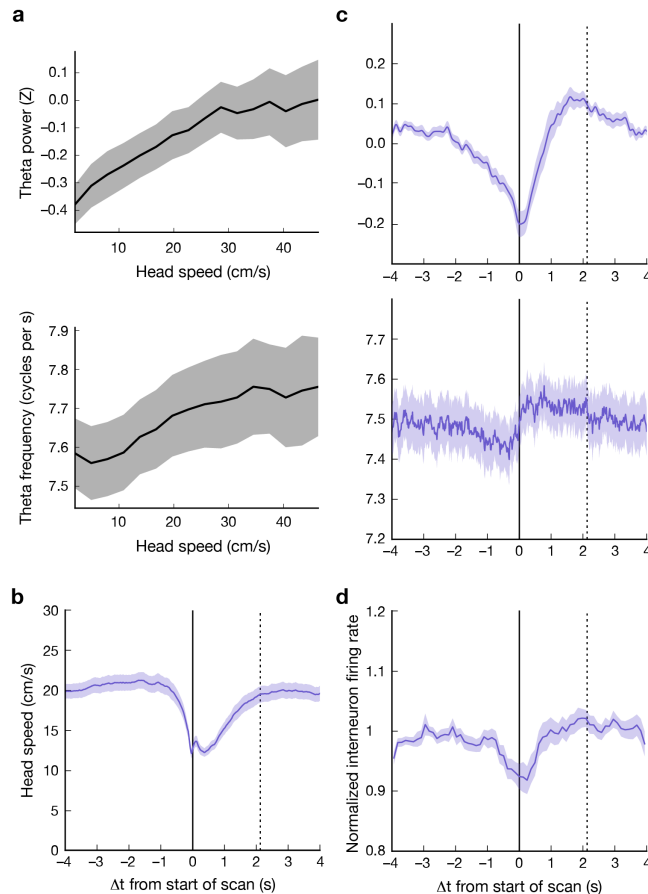
Supplementary Figures



Supplementary Figure 1 | Illustrations of the signal processing steps used to detect head scanning. This figure accompanies the methodological descriptions in Methods/Scanning events. The signal processing for isolating head-scan events is based on four head-motion quantities (**a**) derived from Cartesian (x, y) position data: track angle (α), track-angle velocity ($\dot{\alpha} = d\alpha/dt$), track-centered radius (\bar{r}), and radial velocity ($\dot{r} = d\bar{r}/dt$). Track-angle velocity is used to characterize forward locomotion on the track (**a**, left), while radius and radial velocity are used to characterize lateral head movement (**a**, right). Gray rats: position at time t ; black rats: position at time $t + \Delta t$ for a short interval Δt . The signal processing flow (**b**) iterates across every position data frame (x, y) in a recording session. First, $\dot{\alpha}$ is checked against a running-velocity threshold (10°CW/s , or $\sim 6\text{ cm/s}$) to determine if the animal is running forward around the track. If the current frame is a running frame, then \bar{r} and \dot{r} are added to respective 4 s buffers of lateral movement samples (\bar{r}_{buffer} and \dot{r}_{buffer}) and the iteration continues to the next frame. If not running, then \bar{r} and \dot{r} are checked to see if the position is off-track or if either of the values are significantly outside of their respective buffered distributions of expected lateral movements (Eqns. 5 and 6). If so, the frame is marked as a putative scanning sample and the iteration continues. After the last position frame, the set of scanning samples are processed into head-scan events, which are then filtered (e.g., by minimum duration) to determine the final set of scans.

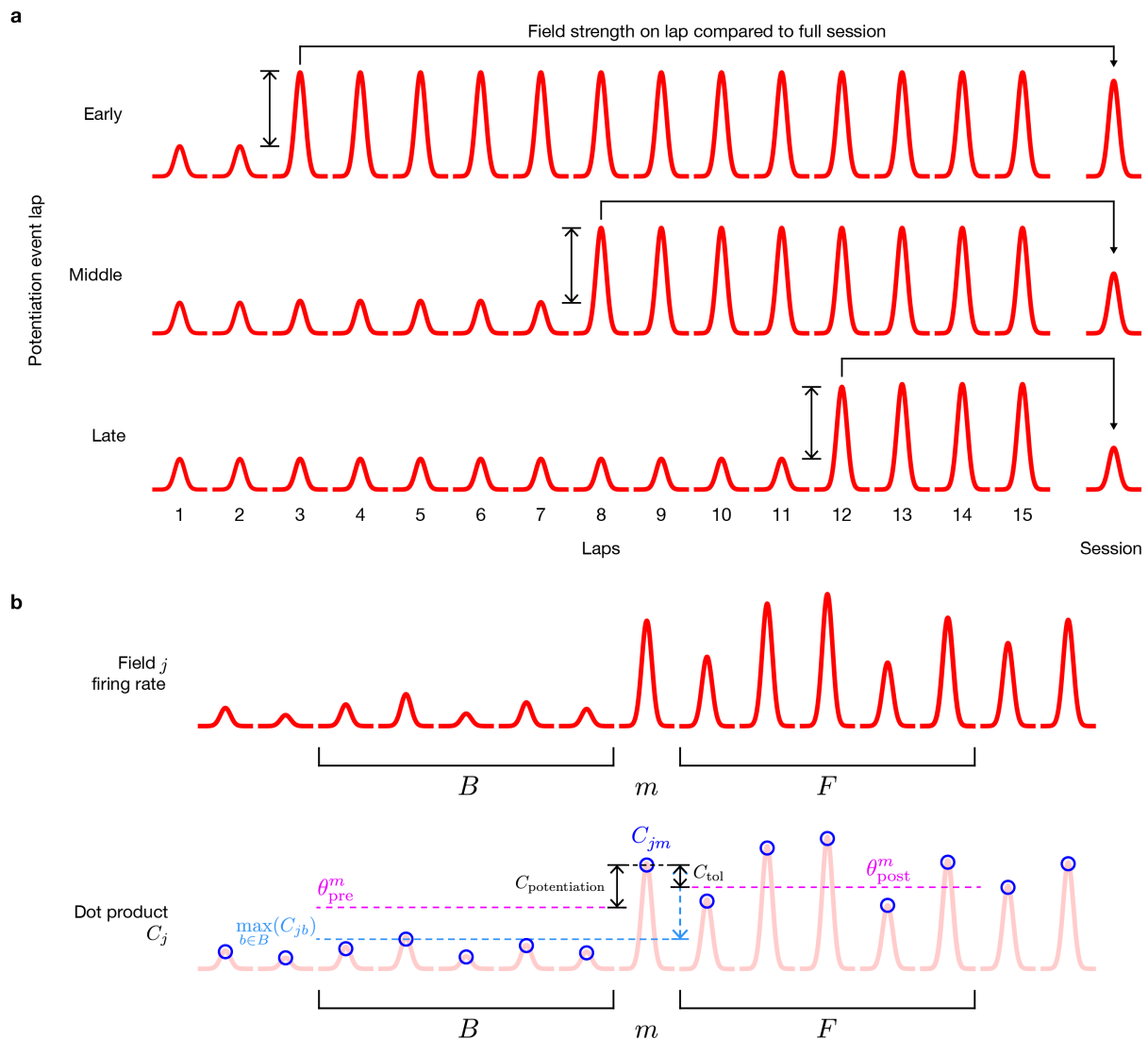


Supplementary Figure 2 | Example scanning events for double cue-rotation and novelty sessions. Additional examples of detected head-scan events (Methods/Scanning events) are shown as highlighted segments (red) of the trajectory (black) across the session. We show examples from different rats performing the double cue-rotation (DR; **a**) and novelty (**b**) experiments.

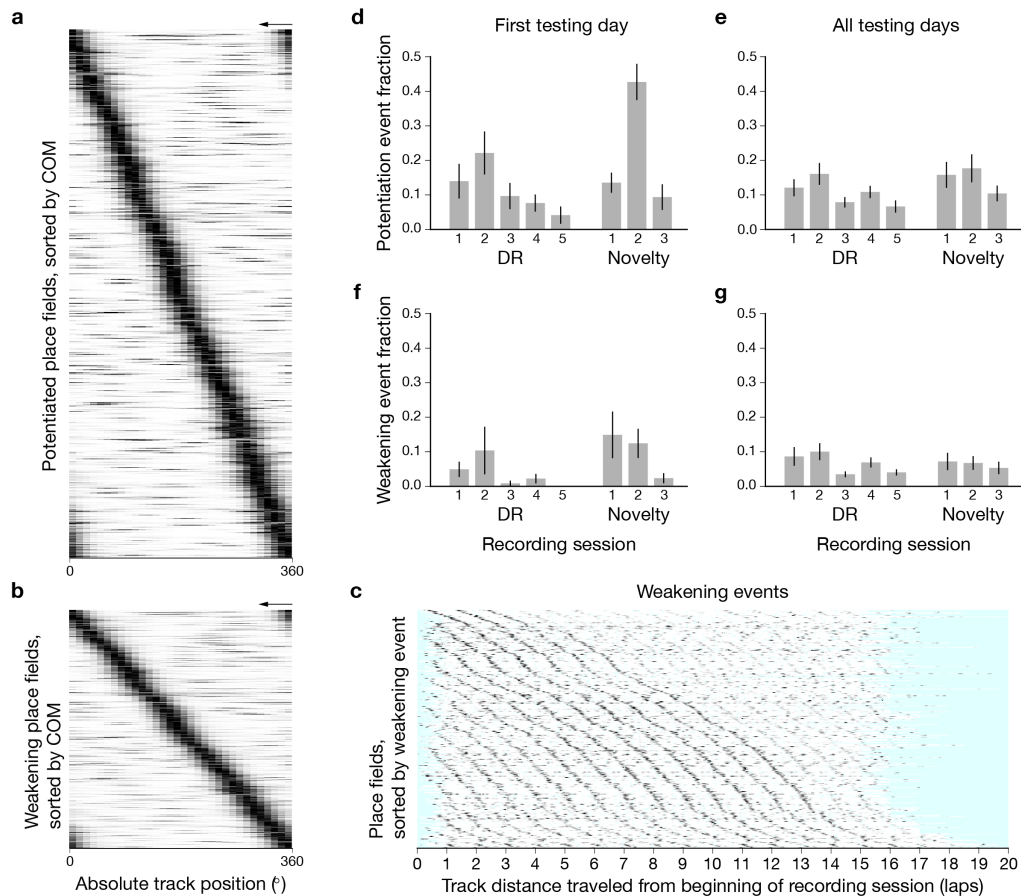


Supplementary Figure 3 | Velocity modulation of local theta and interneuron activity during head scanning.

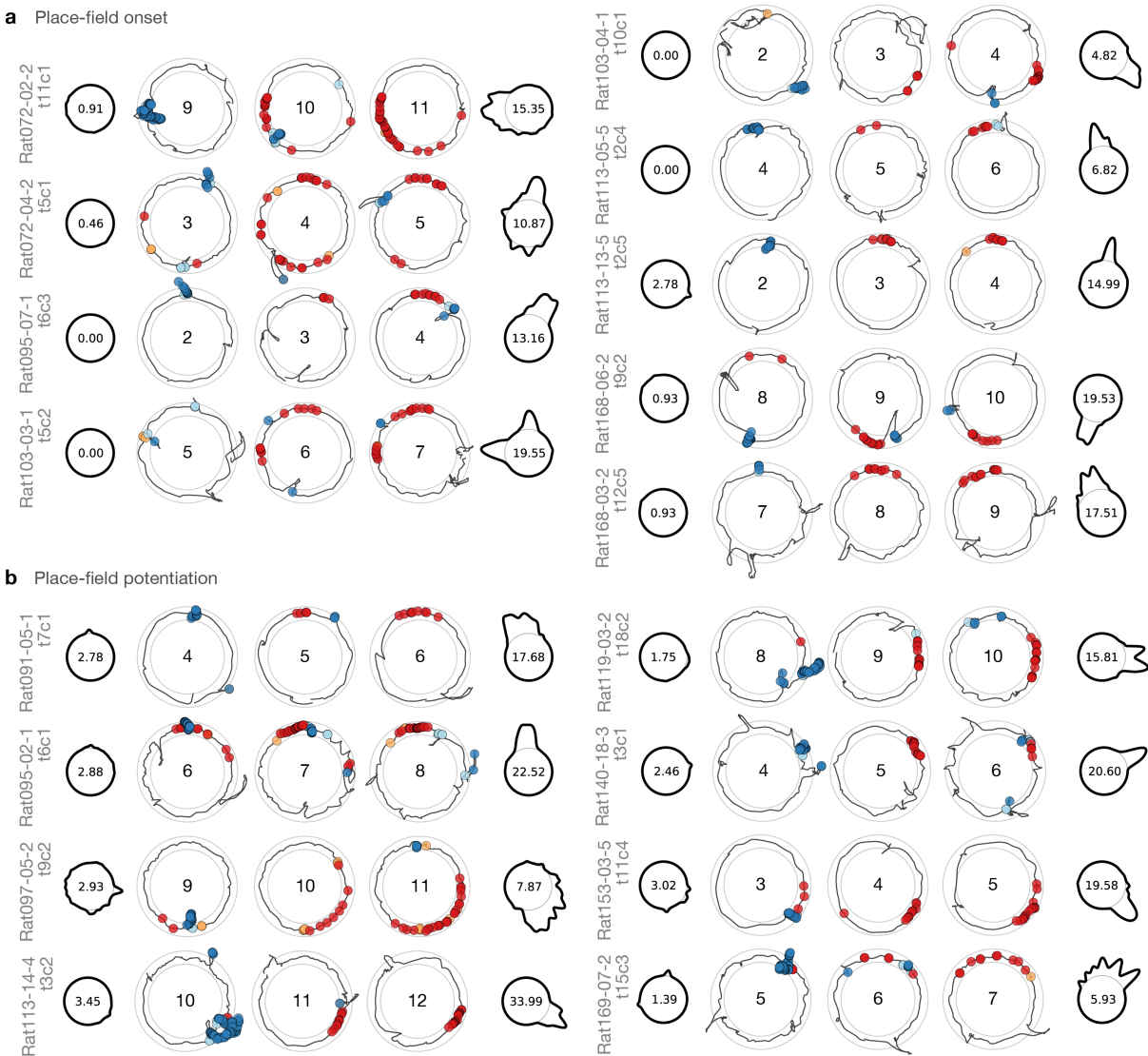
We showed power spectra of CA1 local field potentials (Fig. 1f) demonstrating theta power during head scanning as intermediate between non-scanning pauses and forward running. This result might be explained by velocity-modulation of the local theta rhythm combined with a mixture of slow (pause-like) and faster (running-like) movements of the head and body during scanning. **a**, Velocity-modulation curves for CA1 theta power (top; $n = 21$ rats with CA1 tetrodes) and frequency (bottom) show that increased head speed correlates with higher theta power (two-tailed Friedman test across 16 speed bins, $\chi^2(15, 320) = 133, P = 6.28 \times 10^{-21}$) and higher theta frequency ($\chi^2(15, 320) = 108, P = 3.74 \times 10^{-16}$). Black/gray: mean \pm s.e.m. across rats. **b**, Average head speed sharply drops at the start of scanning and recovers on a time-course approximating the median scan duration (dotted line). **c**, Temporal cross-correlations (mean \pm s.e.m. across rats) of theta power (top) and frequency (bottom) with scan start times show that theta power is sharply reduced, consistent with the pause from running that precedes a scan. Theta recovers strongly within the time-scale of the typical scan. **d**, To address whether interneuron activity was also modulated by scanning, we collected spike trains from 225 interneurons recorded from 19/24 rats with potentiation events. Putative interneurons were identified by high average firing rates and short spike widths. Cross-correlograms for individual cells were normalized by mean firing rate and within-rat averages were median-filtered with a 0.37 s kernel to reduce noise. Interneuron cross-correlations ($n = 19$ rats with interneuron data; mean \pm s.e.m.) demonstrate a moderate reduction in firing rate centered on scan start times. The time-course of head speed is similar to that of reduction in both theta power and interneuron firing rates, suggesting that theta and interneuron activity during scanning are largely controlled by head speed, consistent with observations of other exploratory behaviors.



Supplementary Figure 4 | Illustration of place-field potentiation event detection procedure. This figure is a supplement to the methodological descriptions in Methods/Field potentiation events. The procedure examines the firing within an isolated place field on every lap of the recording session that has at least 2 baseline laps (preceding the test lap) and at least 2 follow-up laps (after the test lap). **a**, The nominal amount of potentiation $C_{\text{potentiation}}$ that we search for is adjusted based on the lap number m of the test lap (i.e., the term $(0.5 + m/N)$ in Eqn. 10) from 50–150% from the start to the end of the session. Illustrated potentiation events of the same size (double arrows) are shown occurring ‘Early’, ‘Middle’, and ‘Late’ within the session to demonstrate why this is necessary. The dot-product measure C_{jm} (Eqn. 9) uses the whole-session firing-rate map (‘Session’) as a stable reference for comparing field strength across laps. However, note that the strength of the session rate-map decreases with later potentiation events due to averaging place-field activity over the session. The lap adjustment in Eqn. 10 counteracts this effective decrease in potentiation threshold. **b**, A more realistic illustration of a place-field potentiation event with variable lap-to-lap activity (top) shows the test lap m , the 5 baseline laps B , and the 5 follow-up laps F . To test lap m for potentiation (bottom), the dot-product strength C_j is computed for every lap (blue circles) and the baseline and follow-up thresholds (magenta lines; Eqns. 10 and 11) are determined relative to the strength C_{jm} of the test lap. The baseline (cyan line) is the maximum field strength of all baseline laps in B . If the baseline is below the potentiation threshold θ_{pre}^m (Eqn. 12) and at least 3 (or 2, if there are only 2) follow-up laps in F are above the persistence threshold θ_{post}^m (Eqn. 13), then lap m is a potentiation event.

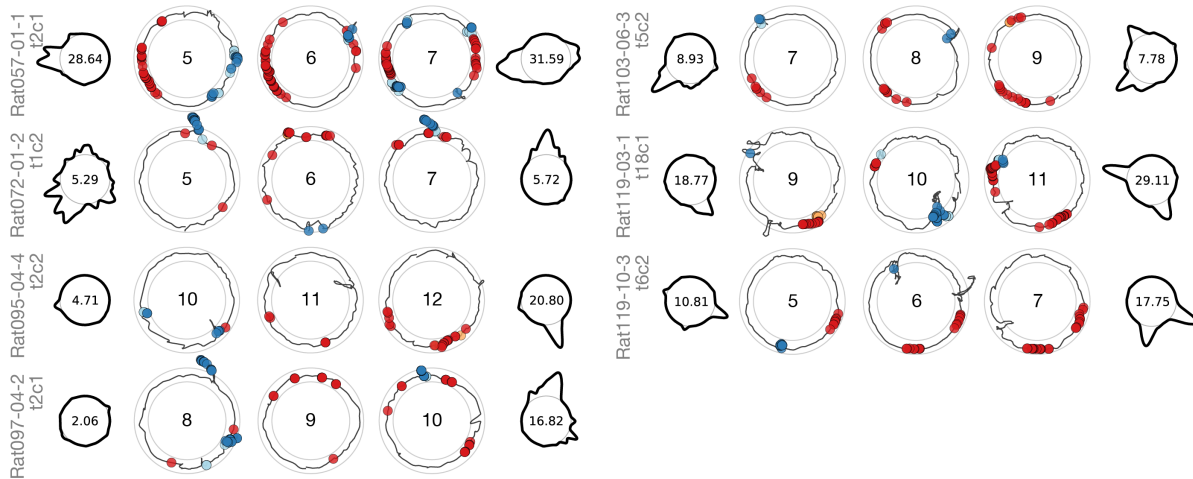


Supplementary Figure 5 | Place-field potentiation and weakening events: Firing-rate maps and prevalence. **a–b**, Linearized firing-rate maps of the whole-session, forward-running activity of potentiated place fields (**a**) and place fields with mid-session ‘weakening’ events (**b**), sorted on the ordinate by track-angle center-of-mass (COM) of each field. **c**, Track-unwrapped firing-rate maps (as in Fig. 2b) of 356 place-fields weakening events (Methods). **d–g**, Event prevalence (mean \pm s.e.m. across rats) is measured as the ratio of potentiation (**d–e**; Supplementary Table 1) or weakening (**f–g**) events to the number of recorded place fields across the 5 DR and 3 novelty sessions. In DR experiments, Sessions 2 and 4 were cue-mismatch configurations; in novelty experiments, Session 2 was the novel room. For the first day of testing (**d**), potentiation prevalence varied significantly across sessions (DR: $n = 14$ rats, two-tailed Friedman test, $\chi^2(4, 65) = 12.3$, $P = 0.0156$; novelty: $n = 6$ rats, $\chi^2(2, 15) = 9.48$, $P = 0.00875$). While the DR experiment showed a general decline in potentiation events across sessions, the novelty experiment showed a sharp increase in the prevalence of potentiation events in the novel session (session 2), consistent with prior reports of abrupt place field formation in novel environments^{23–25}. A similar trend is apparent in Session 2 of the DR experiment, which is the first time that the rats ever experienced the mismatch condition of the otherwise familiar sets of cues. Considering all testing days (**e**), prevalence varied across DR sessions ($n = 20$ rats; $\chi^2(4, 95) = 20.2$, $P = 0.000467$) but showed only a trend in the novelty experiment ($n = 10$ rats; $\chi^2(2, 27) = 5.20$, $P = 0.0743$). Weakening events (**f–g**) occurred less frequently overall than potentiation events, but also varied with session on the first day of the novelty experiment (though without the large increase in Session 2 prevalence observed for potentiation events; **f**, right; $n = 6$ rats, $\chi^2(2, 15) = 6.42$, $P = 0.040$) and across all testing days of the DR experiment (**g**, left; $n = 20$ rats; $\chi^2(4, 95) = 16.5$, $P = 0.00239$).

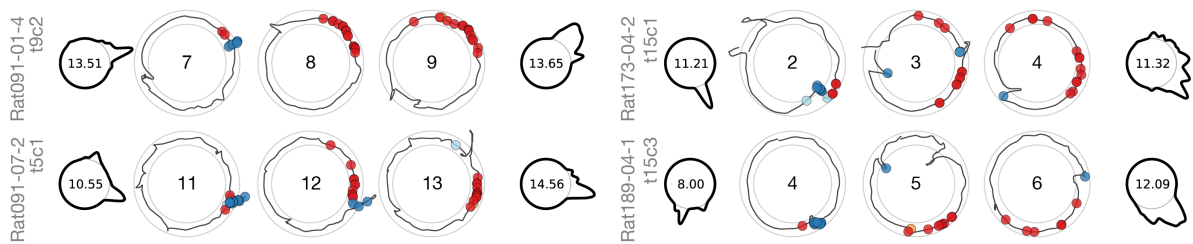


Supplementary Figure 6 | Categorized examples of scan-activated place-field potentiation events. A large selection of significant scan-potential examples are presented to illustrate both the variability of the effect and consistency of the colocalization of scanning activity and subsequent place field changes. Examples are shown using the compact display scheme introduced in Figure 3b, where the left column is a polar firing-rate map of place-field activity on the laps before the predictive scan, the middle three columns show three lap trajectories centered on the potentiation event lap, and the right column is a polar firing-rate map of the place field(s) after the lap following the potentiation event. Peak firing rates (spikes/s) are displayed at the center of polar plots; lap numbers are displayed at the center of lap plots. In lap plots, spike color is behavior-coded: scan (blue), peri-scan (cyan), pause (orange), forward running (red), and other (black). Each example is labeled on the left with the cell identification: e.g., ‘Rat091-05-1 t7c1’ indicates rat subject 91, testing day 5, session 1, tetrode 7, and cell 1. **a**, Place fields that were silent or nearly silent prior to the predictive scan. **b**, Pre-existing but weak fields becoming much stronger after colocalized scanning activity. →

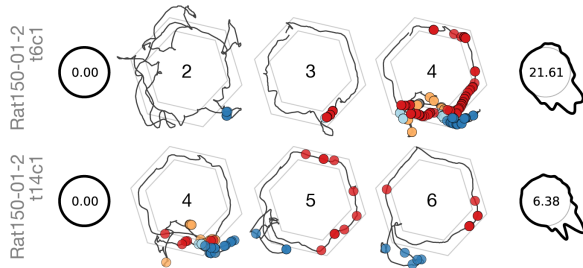
c Addition of secondary place field



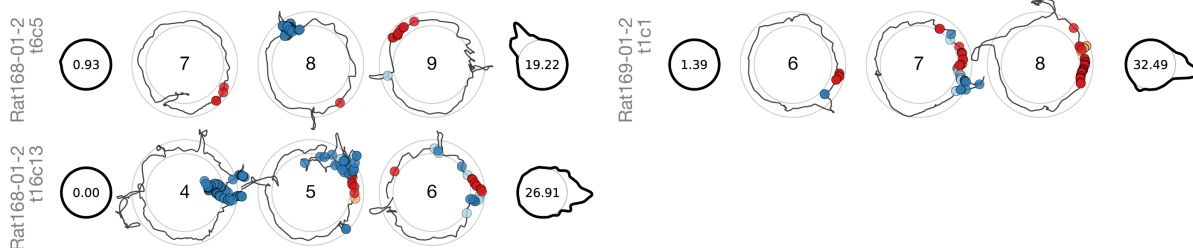
d Counter-clockwise expansion of place field



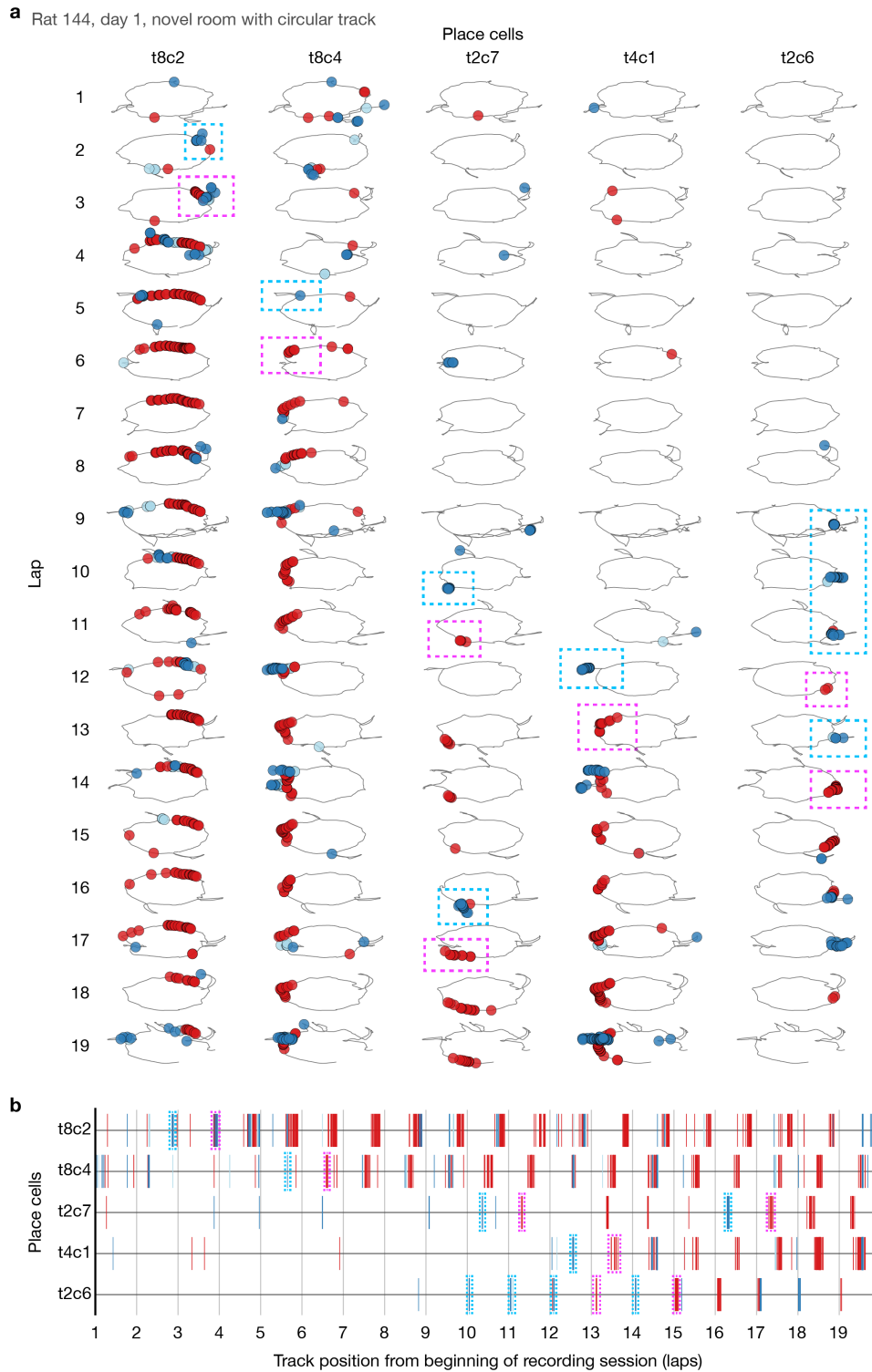
e Simultaneous recording of place-field formation on the hexagonal track during initial exposure to novel room



f Place-field formation in initial exposure to novel room



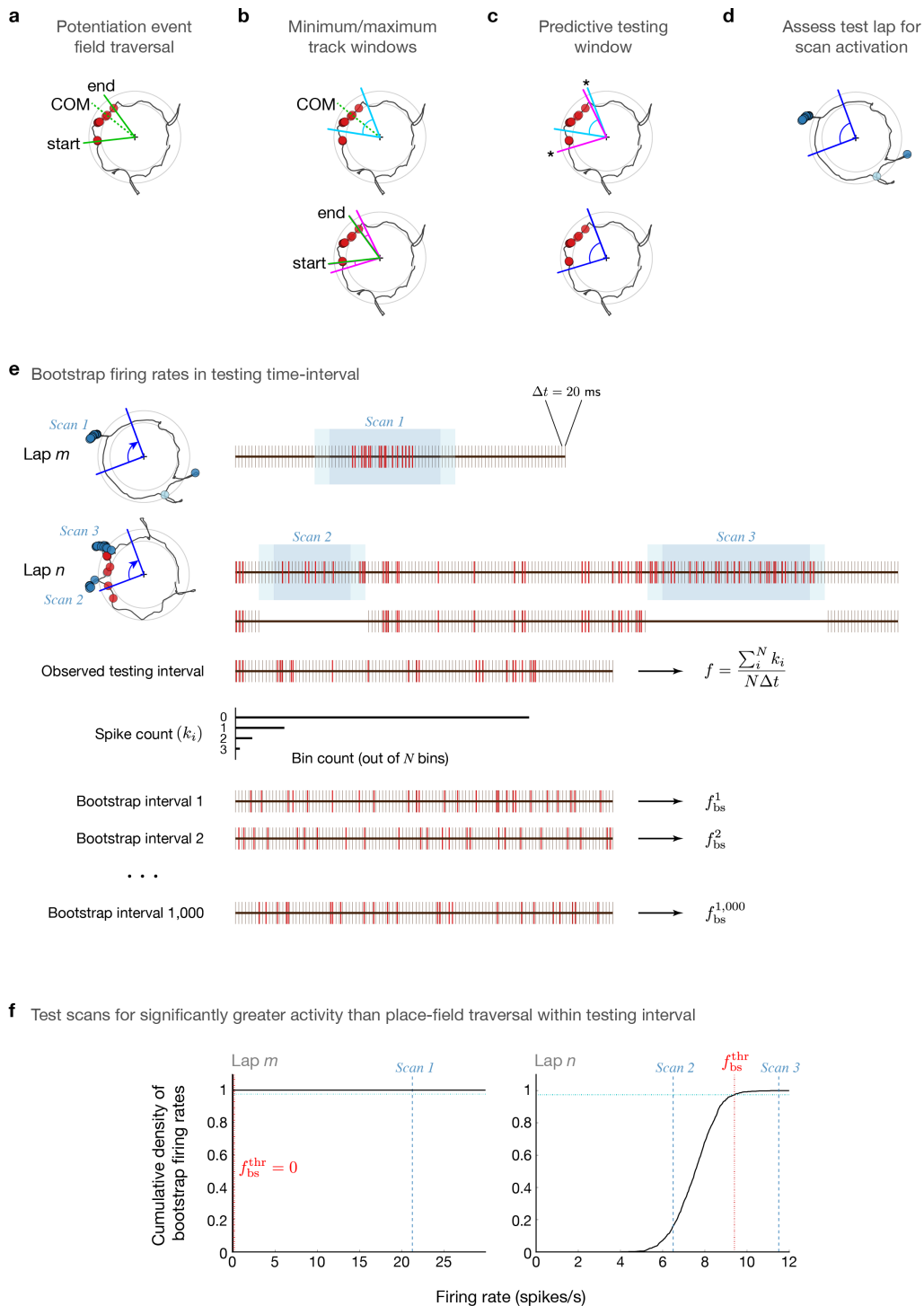
Supplementary Figure 6 (cont'd) | c, Place cells with a pre-existing field developing an additional field at another location. The pre-existing field sometimes weakens or becomes silent, but not always. **d**, Narrow fields that broaden counter-clockwise (CCW) around the track after colocalized scanning activity. **e**, Two simultaneously recorded cells on first exposure to the novel room on the hexagonal track. The top cell forms a new field on lap 3 after a scan on lap 2. Both cells are highly active on a complex scan on lap 4, after which the top cell potentiates and the bottom cell forms a new field. Both fields occur at the same track location. **f**, Additional examples in two other rats of *de novo* scan-activation of place fields on first exposure to the novel room.



Supplementary Figure 7 | Simultaneously recorded place cells form fields activated by scans in the novel room.

An ensemble of 5 place cells from the first day of testing in the novel room demonstrates formation of *de novo* place fields. This is the same ensemble shown in Figure 3d, but here we show the entire recording session (19 laps around the circular track) to provide context for the development of the place fields. We show every place cell for which we detected a potentiation event (out of 13 active place cells recorded during the session), as well as an additional cell ('t2c6') that failed to meet the persistence criteria for potentiation (Eqn. 13) but clearly develops spatially selective firing in the second half of the session. Each detected potentiation event was significantly predicted →

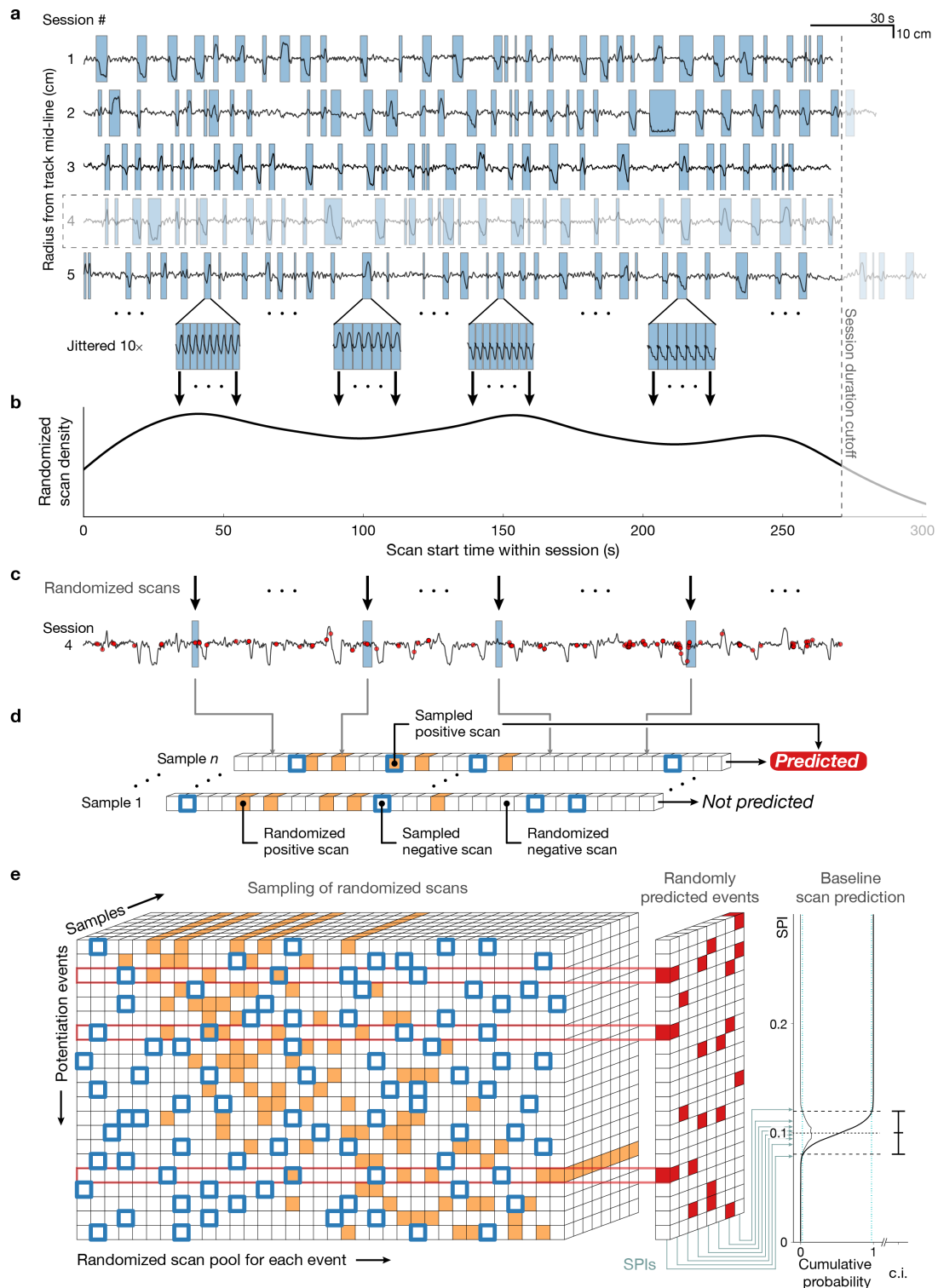
(Supplementary Fig. 8) by colocalized scanning activity on the prior lap. Dashed cyan boxes highlight the predictive scan for each event; dashed magenta boxes highlight the predicted events. Scan (blue), peri-scan (cyan), and forward running (red) spikes are represented with circles (**a**) or tick marks (**b**). The session is shown both as series of trajectory plots for each cell (**a**) as well as raster plots across unwrapped track-angle position from the beginning of the recording session (**b**). The trajectory plots (**a**) are vertically compressed to ensure that cell-lap trajectories are individually discernible. Note that two of the cells ('t2c7' and 't2c6') both have two distinct scan-potential events, where the first event is the initial onset or formation of the field and the second event is a subsequent strengthening and/or broadening of the field. While initial novel-room exposure represents only a minority of our data, these examples (including Supplementary Fig. 6e–f) demonstrate that scan-potential occurs for new fields that develop as the animal becomes familiar with a novel environment.



Supplementary Figure 8 | Illustrations of the predictive scan testing window and test procedure. This figure accompanies Figure 4a and the methodological descriptions in Methods/Scan Prediction Index analysis. **a**, Every potentiation event is defined by the track-angle positions of the first and last spikes (start/end; solid green lines) of the potentiation traversal and by the center-of-mass (COM; dotted green line) of all spikes in the traversal. **b**, Minimum (cyan) and maximum (magenta) track-angle windows (Methods, Eqns. 14 and 15) are defined relative to the COM and start/end, respectively. **c**, We take the outermost bounds of the two windows (asterisks) to form the predictive testing window (blue). **d**, Finally, the test window can be applied to other laps in the session to test whether the amount of scan activity significantly predicts the potentiation event. \rightarrow

e, To test activity on laps (e.g., laps m and n here) for predictive scans, we first check whether the starting track-angle position of any scans fall within the test window on that lap. If not, no further testing is done, and the potentiation event is marked as non-predicted. Otherwise, we test for significantly greater firing during the scans within the window than could be expected by any place-field firing (i.e., firing during forward movement) within the window. We illustrate this process for the within-window scans labeled ‘Scan 1’, ‘Scan 2’, and ‘Scan 3’ on the two laps. First, we determine the time interval corresponding to the test window: the start of the interval is the latest crossing of the leading (CCW) edge of the window, and the end is the earliest crossing of the trailing (CW) edge. The test interval is divided into $\Delta t = 20$ ms bins. The time-lines to the right of laps m and n show bin edges (black ticks), spike times (red ticks), and behavioral epochs (blue/cyan highlights: scan/peri-scan epochs). Lap m only has spiking activity during Scan 1, but lap n has both scan and place-field activity. Considering the lap n activity, the test interval is filtered to remove scan and pause behaviors. The result is the ‘Observed testing interval’, which is a set of N time bins with corresponding spike counts k_i for each bin i , producing a spike-count distribution (histogram). The firing rate f of the interval is computed as the sum of spike counts across bins divided by the total duration of the bins. Next we construct a bootstrap distribution of firing rates. For 1,000 iterations, we bootstrapped the test interval by randomly sampling with replacement the observed spike-count distribution for N time bins. Several bootstrap intervals are illustrated for example. The firing rates f_{bs}^j of these bootstrap intervals constitute the expected firing-rate distribution used to test the significance of scan firing.

f, We show the cumulative density functions for the lap m (left) and lap n (right) expected firing-rate distributions. The upper bound of the expected 95% c.i. corresponds to the 97.5 percentile (cyan dotted line) and is used as the minimum threshold (f_{bs}^{thr} ; red dotted line) for significance of the scan firing (Eqn. 16). Lap m had no place-field activity, thus its expected distribution and significance threshold are both 0 (left). Scan 1 had a non-zero firing rate (blue dashed line) and would thus be counted as a predictive scan for the place-field potentiation event in question. Lap n had expected place-field firing rates centered ~ 7.5 spikes/s (black curve) and a corresponding threshold ~ 9.4 spikes/s (right). Scan 2 is below threshold and thus not significant, while Scan 3 is above threshold and would be counted as predictive. The Scan Prediction Index analysis examines the proportion of scan-predicted potentiation events by testing the lap prior to the event.



Supplementary Figure 9 | Procedure for generating expected distributions for the Scan Prediction Index. This figure is a supplement to Figure 4b–c, Figure 5a–e, Supplementary Figure 10a–d, and the methodological descriptions in Methods/Scan Prediction Index analysis. We used a Monte Carlo randomization and resampling process to generate expected SPI distributions, which is illustrated here for an example DR dataset (rat subject 95, testing day 4). →

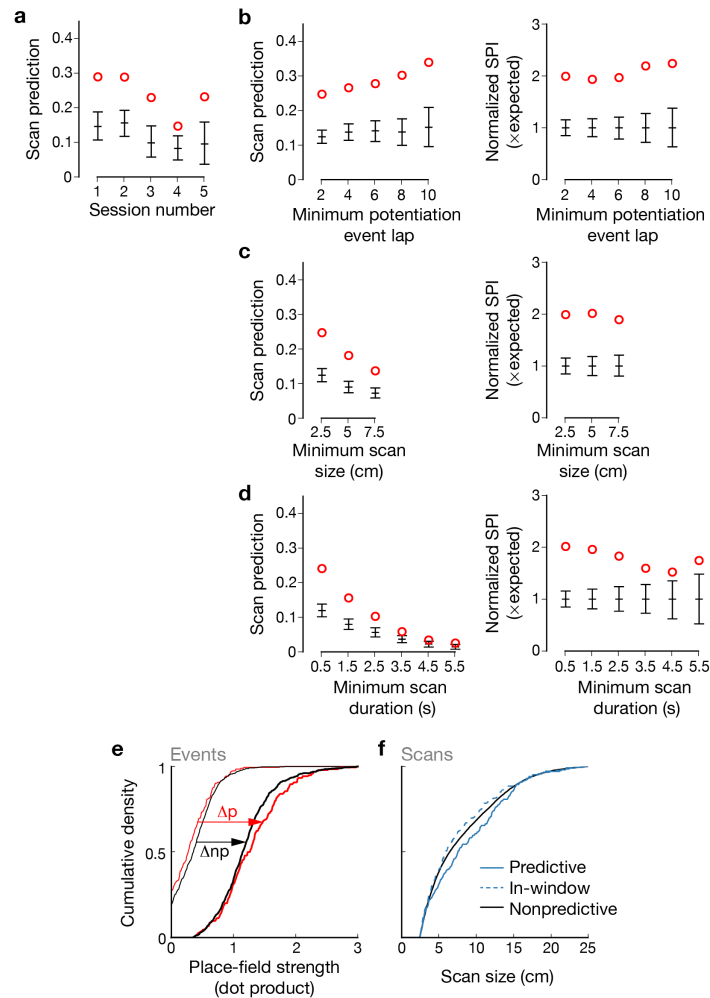
a, We show time-series for each session in the example dataset of radial distance from the track mid-line where scan events are highlighted (blue). Supposing that session 4 (dashed box, dimmed) contains the potentiation event for which we are creating expectations, we collect the start times (relative to the start of the session) and durations for all scan events in the other sessions (i.e., 1, 2, 3, and 5).

b, We create a pool of randomized scans by adding each non-event-session scan to the pool 10 times with up to 10 s of uniform random jitter. Any randomized scans that extend beyond the duration of the event session are excluded ('Session duration cutoff'). The resulting temporal distribution (black curve) can be sampled to generate randomized scan trains that preserve the scanning characteristics for that animal on that testing day.

c, Each randomized scan in the pool (arrows: examples) is assigned the spike count from the corresponding scan interval within the event-session spike train (session 4, red circles). Randomized scans are allowed to overlap with actual scan intervals from the event session.

d, The randomized scans are tested for predictiveness as usual (Supplementary Fig. 8), with the results illustrated as an array representing the randomized scan pool: scans test positive (orange) or negative (white). We randomly choose the number of scans observed during the event session (blue outlines), which is session 4 in this example. If no positive scans are chosen (as in Sample 1), then the random sample is considered non-predicted; if at least one positive scan is chosen (as in Sample n), then the sample is considered predicted.

e, For all potentiation events for which we are computing a baseline, we illustrate the random sampling process as a 3-dimensional matrix (left) with potentiation events, the randomized scan pools, and random samples along the axes. The front face of this matrix shows a single random sample, where positive predictive scans (orange) can be randomly selected (blue outlines) for each potentiation event. Some potentiation events (red outlines) selected a positive scan and are considered to be randomly predicted. For each of 5,000 samples, we collected the set of events that are randomly predicted in a 2-dimensional matrix (middle). The fraction of randomly predicted events in each column is the expected SPI (Eqn. 17) for the corresponding random sample. We use the distribution of these SPIs (right) to calculate the mean and empirical 95% confidence interval (c.i., error bar). The c.i. constitutes the chance expectation for the scan-potentiation effect. We consider the observed predictiveness to be significant if it is greater than the upper bound of the chance expectation.



Supplementary Figure 10 | Marginal and *post hoc* analysis of the scan-potential effect. This figure is a supplement to Figure 5 which presents the primary results of the SPI analysis. **a–d**, We show additional SPI data points (red circles) along with the corresponding expected random baselines (black bars: mean and 95% c.i.). **a**, SPIs across experimental session number (both experiments combined). **b–d**, Minimum thresholds are applied to select the potentiation events (**b**) or scans (**c–d**) that contribute to predictive tests. For these plots, the right panel shows the same data but normalized to the expected chance value. SPIs increase when restricting analysis to later laps, but not relative to expected values (**b**). While restricting analysis to larger (**c**) or longer (**d**) scans reduces overall predictiveness, the effect remains significantly above baseline up to 1.5–2× the expected values. **e**, *Post hoc* comparisons of predicted and nonpredicted events. Distributions are displayed as cumulative density functions. We constructed *post hoc* event distributions by dividing field potentiation events into positively predicted events and nonpredicted events. Predicted events (red; Δp) underwent stronger total potentiation ($n = 195$ events, 0.982 ± 0.521 , mean \pm s.d.) than nonpredicted events (black, Δnp ; $n = 594$ events, 0.836 ± 0.442 ; two-tailed, two-sample Kolmogorov-Smirnov test, $D = 0.163$, $P = 0.000685$), where total potentiation was defined as the dot-product field strength of the potentiated traversal minus the maximum field strength of the event’s baseline laps. This difference resulted from a trend toward weaker baselines (thin lines; $D = 0.109$, $P = 0.0549$) and significantly stronger potentiated fields (thick lines; $D = 0.128$, $P = 0.0152$) for predicted events compared to nonpredicted events. **f**, *Post hoc* comparisons of predictive and nonpredictive scans. We constructed *post hoc* scan distributions by dividing all of the scans from the recording sessions of every potentiation event into those that tested positive for the event, those that tested negative but were within the event testing window, and the remaining non-predictive scans. Predictive scans (solid blue; $n = 214$) were larger than nonpredictive scans that occurred both within (dashed blue; $n = 264$ scans; $D = 0.149$, $P = 0.00901$) and outside of (black; $n = 27,631$ scans; $D = 0.105$, $P = 0.0168$) the testing window.

Supplementary Tables

Supplementary Table 1 | Prevalence of field potentiation events across hippocampal place fields.

Category	Value	Potentiation Events	/	Place Fields	Event Fraction
Subregion	CA1	608	/	3,439	0.1768
	CA3	181	/	2,071	0.0874
Testing Day	1	106	/	599	0.1770
	2	76	/	658	0.1155
	3	115	/	805	0.1429
	4	92	/	829	0.1110
	5	102	/	659	0.1548
	6	96	/	613	0.1566
	7	77	/	544	0.1415
	8	71	/	429	0.1655
Session Type	STD	338	/	2,911	0.1161
	MIS	332	/	1,767	0.1879
	FAM	67	/	560	0.1196
	NOV	52	/	272	0.1912
DR Session	1	154	/	931	0.1654
	2	187	/	834	0.2242
	3	98	/	960	0.1021
	4	143	/	906	0.1578
	5	82	/	991	0.0827
Mismatch Angle	45°	67	/	421	0.1591
	90°	96	/	440	0.2182
	135°	87	/	469	0.1855
	180°	80	/	424	0.1887
Novelty Session	1	43	/	278	0.1547
	2	52	/	272	0.1912
	3	24	/	282	0.0851
Rat	057	19	/	180	0.1056
	064	4	/	50	0.0800
	072	90	/	870	0.1034
	087	0	/	8	0.0000
	091	27	/	210	0.1286
	095	75	/	400	0.1875
	097	58	/	420	0.1381
	103	86	/	344	0.2500
	113	94	/	573	0.1640
	114	15	/	91	0.1648
	119	137	/	779	0.1759
	137 [†]	3	/	25	0.1200
	138 [†]	0	/	33	0.0000
	139 [†]	7	/	21	0.3333
	140 [†]	7	/	37	0.1892
	144 [†]	23	/	169	0.1361
	150 [†]	15	/	91	0.1648
	153	4	/	69	0.0580
	157 [†]	1	/	30	0.0333
	160 [†]	10	/	59	0.1695
	168 ^{†*}	57	/	436	0.1307
	169 ^{†*}	38	/	298	0.1275
	173	3	/	51	0.0588
189	2	/	29	0.0690	
195	12	/	121	0.0992	
197	0	/	83	0.0000	
227	2	/	28	0.0714	
232	0	/	5	0.0000	
Overall	—	789	/	5,510	0.1432

[†] Rats tested in the novelty experiment

^{†*} Rats tested in the novelty and DR experiments